Journal of Coordination Chemistry

ISSN: 0095-8972 (Print) 1029-0389 (Online) Journal homepage: http://www.tandfonline.com/loi/gcoo20

Axial coordination of pyridyl-containing pentacenes to porphyrins

Andreas R. Waterloo, Rainer Lippert, Norbert Jux & Rik R. Tykwinski

To cite this article: Andreas R. Waterloo, Rainer Lippert, Norbert Jux & Rik R. Tykwinski (2015) Axial coordination of pyridyl-containing pentacenes to porphyrins, Journal of Coordination Chemistry, 68:17-18, 3088-3098, DOI: 10.1080/00958972.2015.1057711

To link to this article: http://dx.doi.org/10.1080/00958972.2015.1057711

Accepted author version posted online: 03 Jun 2015.
Published online: 02 Jul 2015.

Journal of Coordination Chemistry, 2015
Vol. 68, Nos. 17–18, 3088–3098, http://dx.doi.org/10.1080/00958972.2015.1057711

Axial coordination of pyridyl-containing pentacenes to porphyrins

ANDREAS R. WATERLOO, RAINER LIPPERT, NORBERT JUX* and RIK R. TYKWINSKI*

Department of Chemistry and Pharmacy & Interdisciplinary Center for Molecular Materials (ICMM), University of Erlangen-Nürnberg (FAU), Erlangen, Germany

(*Received 4 April 2015; accepted 23 April 2015*)

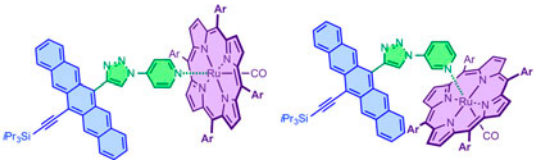

A pair of pentacenes that are functionalized in the 6-position with either a 3- or 4-pyridyl group via a triazole linker have been used to form complexes with a tetra(aryl)ruthenium(II) porphyrin through axial coordination. The pentacene–porphyrin dyads **5** and **6** have been structurally characterized through a combination of spectroscopic techniques. UV–vis spectroscopy shows that the absorption profiles of the two chromophores, the porphyrin and the pentacene, are complementary, providing absorptions throughout the UV and visible regions. While the dyads are reasonably stable in the solid state under ambient conditions they are, unfortunately, only stable in solution for hours when exposed to light and air.

Keywords: Functionalized pentacene; Axial coordination; Porphyrin; CuAAC reaction

1. Introduction

Metal–pyridine complexation has been extensively used in coordination chemistry [1], especially in the formation of porphyrin-containing architectures [2–4]. Axial complexation of pyridyl moieties to metalloporphyrin centers can lead to supramolecular assemblies such as cages [5], oligomers [6], polymers [7], wires [8], or tweezers [9]. Complementing the intriguing properties of porphyrins are those of polycyclic aromatic hydrocarbons such as pentacenes. While unsubstituted pentacene is relatively unstable under ambient conditions and only sparingly soluble in common organic solvents [10], substituted pentacenes have recently emerged as a versatile platform to provide a range of useful molecular materials.

*Corresponding authors. Email: norbert.jux@fau.de (N. Jux); rik.tykwinski@fau.de (R.R. Tykwinski)
Dedicated to Professor Rudi van Eldik on the occasion of his 70th birthday.

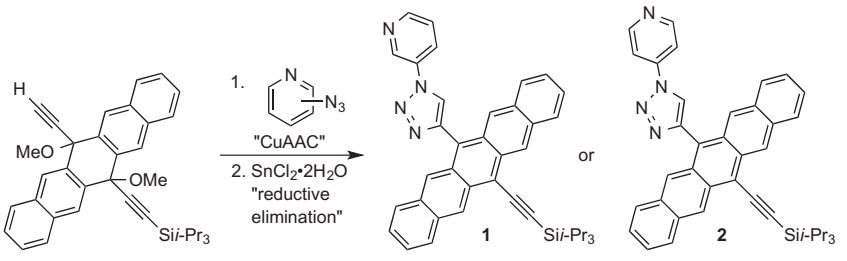

Figure 1. Pyridyl-containing pentacenes **1** and **2** formed by CuAAC [16].

As a result, acenes have been widely studied as high-performance organic semiconductors [11–14].

We have recently shown that the Cu(I)-catalyzed alkyne–azide cycloaddition (CuAAC) [15] offers a possibility to easily alter the substitution pattern of 6,13-disubstituted pentacenes under mild reaction conditions [16]. In addition to allowing the incorporation of aryl and alkyl groups, the CuAAC allowed for the introduction of pyridyl moieties onto the pentacene framework, as in **1** and **2** (figure 1) [16]. It was hypothesized that a combination of pyridyl-containing pentacene derivatives **1** and **2** and a metalloporphyrin via axial coordination could lead to pentacene–porphyrin dyads with potentially interesting electronic and/or optical properties, based on the complementary chromophores of the two components of the dyad [17]. The results of this study are reported herein.

2. Experimental

2.1. *Materials and methods*

Compounds **1** [16], **2** [16], and **3** [18] were synthesized as reported. Chemicals were purchased in reagent grade from commercial suppliers and used without purification. Unless otherwise stated, all reactions were performed in standard, dry glassware under nitrogen. All solvents were dried and/or distilled prior to use. Dry, deoxygenated methylene chloride was distilled from calcium hydride; dry, deoxygenated hexanes were distilled from sodium.

NMR spectra were recorded on a Bruker Avance 300 operating at 300 MHz (^{1}H NMR) and 75 MHz (^{13}C NMR) or on a Bruker Avance 400 operating at 400 MHz (^{1}H NMR) and 100 MHz (^{13}C NMR) at rt. The signals were referenced to residual solvent peaks (δ in parts per million; ppm). Coupling constants are reported as observed (±0.5 Hz). For simplicity, the coupling constants for the aryl protons of *para*-substituted aryl groups have been reported as pseudo first order (i.e. doublets), even though they are second-order (AA′XX′) spin systems. Mass spectra were obtained from a Bruker Daltonik maXis 5G UHR ESI-TOF instrument. IR spectra were recorded on a Varian-660 IR spectrometer in ATR mode. UV–vis absorption spectra were acquired at rt using a Varian Cary 5000 spectrophotometer; λ_{max} in nm (ε in L mol^{-1} cm^{-1}).

2.2. *Synthesis*

2.2.1. Pyridine-porphyrin dyad 4. Ru*t*BuPP·H_2O **3** (50 mg, 0.050 mmol) was dissolved in dry methylene chloride (10 mL). Dry pyridine (5 mL) was added and the reaction

mixture was stirred under ambient conditions for 3 h at rt. The reaction solution was evaporated to dryness, and the residue was precipitated from chloroform/pentane to provide **4** as a red solid (50 mg, 95%). IR (ATR): 3026 (w), 2957 (s), 2865 (s), 1946 (s), 1006 (s), 792 (s), 713 (s) cm^{-1}; UV–vis (CH_2Cl_2) λ_{max} (ε): 245 (25 500), 415 (111 000), 534 (11 500), 569 (6 000) nm; ^1H NMR (300 MHz, C_6D_6): δ 9.02 (s, 8H), 8.21 (d, J = 9.8 Hz, 4H), 8.18 (d, J = 9.9 Hz, 4H), 7.59 (d, J = 7.9 Hz, 4H), 7.54 (d, J = 7.9 Hz, 4H), 4.96 (t, J = 7.5 Hz, 1H), 4.36 (t, J = 7.3 Hz, 2H), 1.88 (d, J = 5.1 Hz, 2H), 1.42 (s, 36H); ^{13}C NMR (75 MHz, C_6D_6): δ 181.4, 150.5, 145.0, 144.6, 140.8, 135.4, 134.7, 133.0, 124.4, 123.8, 122.8, 121.6, 35.0, 31.9; ESI HRMS (CH_2Cl_2/MeCN) Calcd for $C_{66}H_{65}N_5O^{102}Ru$ ($[M]^+$) m/z 1045.4227, found 1045.4256.

2.2.2. Synthesis of pentacene–porphyrin dyads 1 and 2.

2.2.2.1. *General procedure.* A Schlenk flask was charged with either pyridyl-substituted pentacene derivative **1** or **2** (1 equiv) and Ru*t*BuPP·H_2O **3** (1 equiv). Dry, deoxygenated benzene (5 mL) was added and the solution was stirred for 1 h at rt. The mixture was heated to 50 °C and stirred for 2 h at that temperature. The reaction mixture was cooled to rt and the solvent was removed under reduced pressure. The solid purple residue was redissolved in minimal amount of dry, deoxygenated methylene chloride and precipitated by addition of a large amount of dry, deoxygenated hexanes. The solids were filtered under N_2 and dried *in vacuo* to provide the products as purple solids.

2.2.2.2. *Dyad 5.* Pentacene **1** (12 mg, 0.020 mmol) and Ru*t*BuPP·H_2O **3** (20 mg, 0.020 mmol) were used according to the *General Procedure*. Complex **5** was obtained as a purple solid (21 mg, 67%). M.p. > 400 °C; UV–vis (CH_2Cl_2) λ_{max} (ε): 309 (210 000), 346 (13 300), 415 (200 000), 496 (5 350), 534 (18 700), 571 (11 400), 622 (11 600) nm; IR (ATR): 3029 (w), 2953 (s), 2862 (s), 2123 (m), 1949 (s), 1262 (s), 1006 (s) cm^{-1}; ^1H NMR (300 MHz, C_6D_6): δ 9.70 (s, 2H), 9.05 (s, 8H), 8.43 (s, 2H), 8.38 (d, J = 2.0 Hz, 2H), 8.35 (d, J = 2.0 Hz, 2H), 8.11 (d, J = 2.0 Hz, 2H), 8.09 (d, J = 1.9 Hz, 2H), 7.99 (d, J = 8.7 Hz, 2H), 7.53–7.40 (m, 11H), 7.31 (d, J = 2.1 Hz, 2H), 7.29 (d, J = 2.1 Hz, 2H), 6.80 (s, 1H), 5.62 (d, J = 8.2 Hz, 1H), 4.30 (dd, J = 8.3, 5.7 Hz, 1H), 2.42 (d, J = 2.4 Hz, 1H), 1.95 (dd, J = 5.7, 1.2 Hz, 1H), 1.46–1.45 (m, 21H), 1.34 (s, 36H). ESI HRMS (CH_2Cl_2/MeOH) Calcd for $C_{101}H_{98}N_8O^{102}RuSi$ ($[M]^+$) m/z 1568.6676, found 1568.6715; Calcd for $C_{61}H_{60}N_4RuO$ ($[M–\mathbf{1}]^+$) m/z 966.3822, found 966.3830.

2.2.2.3. *Dyad 6.* Pentacene **2** (10 mg, 0.017 mmol) and Ru*t*BuPP·H_2O **3** (17 mg, 0.017 mmol) were used according to the *General Procedure*. Complex **6** was obtained as a purple solid (20 mg, 74%). UV–vis (CH_2Cl_2) λ_{max} (ε): 309 (133 000), 348 (8 200), 415 (125 000), 496 (3 420), 534 (11 600), 571 (7 100), 622 (7 300) nm; IR (ATR): 2955 (s), 2863 (s), 1966 (s), 1609 (s), 1350 (s), 1006 (s), 715 (s) cm^{-1}; ^1H NMR (300 MHz, C_6D_6): δ 9.62 (s, 2H), 9.10 (s, 8H), 8.43 (d, J = 2.0 Hz, 2H), 8.40 (d, J = 2.0 Hz, 2H), 8.27 (s, 2H), 8.22 (d, J = 2.0 Hz, 2H), 8.20 (d, J = 2.0 Hz, 2H), 7.90 (d, J = 8.4 Hz, 2H), 7.68 (d, J = 2.0 Hz, 2H), 7.65 (d, J = 2.0 Hz, 2H), 7.59 (d, J = 2.0 Hz, 2H), 7.56 (d, J = 2.1 Hz, 2H), 7.51 (d, J = 8.4 Hz, 2H), 7.03–6.88 (m, 5H), 6.30 (s, 1H), 4.72 (d, J = 7.1 Hz, 2H), 1.86 (d, J = 7.1 Hz, 2H), 1.42 (bs, 36H), 1.37–1.36 (m, 21H); ESI HRMS (CH_2Cl_2/MeOH) Calcd for $C_{101}H_{98}N_8O_2{}^{102}RuSi$ ($[M–CO + MeOH]^+$) m/z 1572.6620, found 1572.6989.

3. Results and discussion

3.1. *Synthesis of pyridine-porphyrin complex*

The synthesis envisioned for the desired porphyrin complexes would rely on a ligand exchange reaction with Ru(II)-porphyrin **3** [18]. The use of *tert*-butyl substitution in the *para*-position of the porphyrin should help to ensure solubility of the products, and it has been shown previously that the nature of the aryl substituent in the *meso*-position has little impact on the optical characteristic of the Ru-porphyrin, due to the orthogonal conformation of the aryl rings [18]. For comparison and as reference compound, the pyridine complex of Ru(II)-porphyrin **3** was generated first. To this end, Ru(II)-porphyrin **3** was dissolved in methylene chloride and treated with excess of pyridine (scheme 1). After work up, the desired pyridine complex **4** was isolated in excellent yield (95%). The solubility of pyridine complex **4** is remarkably increased compared to ruthenium porphyrin **3**.

3.2. *Characterization of pyridine-porphyrin complex*

The ^{1}H NMR spectrum of **4** is shown in figure 2. The protons of the coordinated pyridine are strongly shifted to higher field due to the diamagnetic anisotropy of the porphyrin, as reported for other pyridyl Ru-porphyrin dyads [2]. The *ortho*-protons of the pyridine moiety are most affected by the porphyrin ring and resonate as a doublet at 1.88 ppm, while the *meta*- and *para*-protons of the coordinated pyridine appear as triplets at 4.36 ppm and 4.96 ppm, respectively. Restricted rotation of the 4-*tert*-butylphenyl groups of the porphyrin is observed for both metalloporphyrin **3** and **4**. As a result of the unsymmetrical faces of the porphyrin, the two sets of *ortho* and *meta* aryl protons are chemical shift inequivalent and show as independent doublets rather than an AA′BB′ system that would result from free rotation about the aryl–porphyrin bond.

The ^{13}C NMR spectrum of **4** reveals 14 of the expected 15 signals. The three signals for the coordinated pyridine ring are at 144.6 ppm (*ortho*), 135.4 (*para*) and 121.6 ppm (*meta*). The carbon of the coordinated carbonyl group resonates at 181.3 ppm, and the ^{13}C NMR spectrum shows unique resonance for five of the six unique carbons of the 4-*tert*-butylphenyl groups. Finally, the C=O vibrational band at 1946 cm^{-1} dominates the IR spectrum of **4**, very similar to that found in other analogous pyridyl Ru-porphyrin complexes [2b].

The UV–vis spectrum of **4** is depicted in figure 3. The spectrum shows the typical three bands for a metalloporphyrin, namely the intense Soret-Band of the porphyrin at 415 nm,

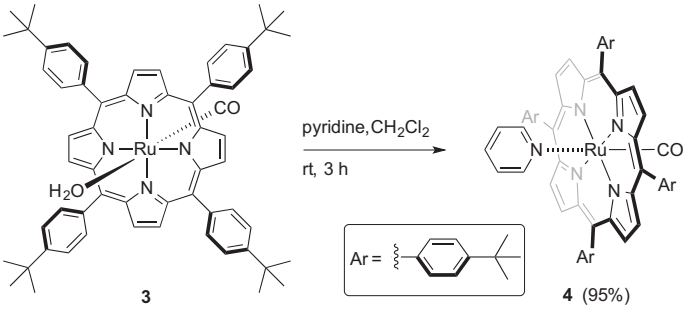

Scheme 1. Synthesis of pyridine-porphyrin complex **4**.

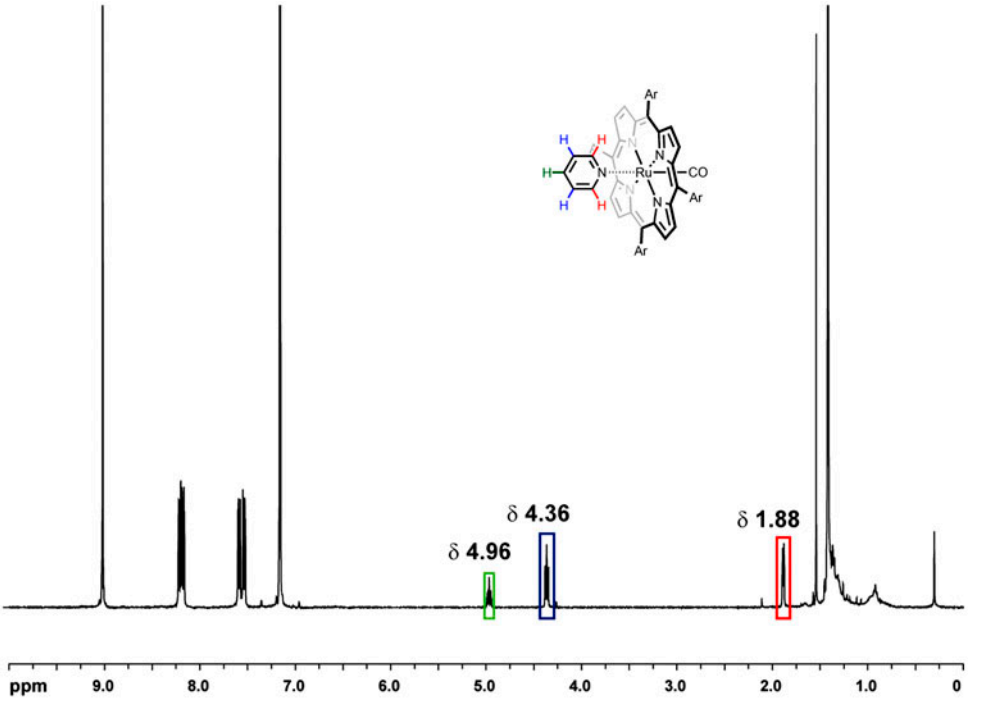

Figure 2. ^{1}H NMR spectrum (300 MHz, C_6D_6) of **4**. The resonances assigned to the pyridyl protons are highlighted.

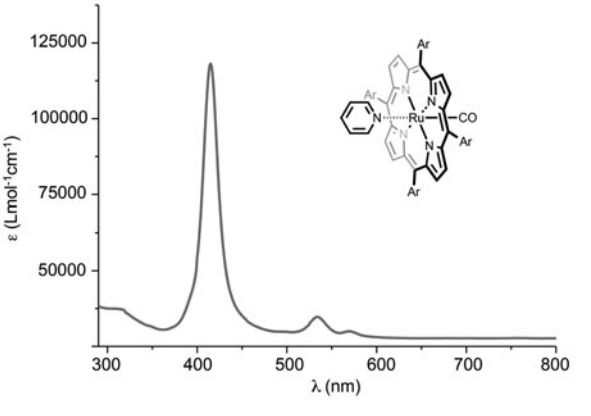

Figure 3. UV–vis spectrum of **4** in CH_2Cl_2.

and the two Q-bands at 534 nm and 569 nm. These signals are virtually unchanged from those of other reported Ru(II)-tetra(aryl)porphyrins with axial ligands, which show analogous absorptions at *ca.* 415, 532, and 565 nm, regardless of substitution pattern about the porphyrin [2, 18].

3.3. *Synthesis of pentacene–porphyrin dyads*

The combination of porphyrin **3** with the pentacene derivatives **1** and **2** was then explored. Thus, **1** was dissolved in benzene along with a stoichiometric amount of Ru(II)-porphyrin **3** (scheme 2) and the solution stirred at room temperature for an hour. The solution was then heated to 50 °C and allowed to react for an additional 2 h. After cooling and removal of the solvent, the resulting purple residue was dissolved in minimal dry, deoxygenated methylene chloride and precipitated by the addition of a large amount of dry, deoxygenated hexanes. This gave the pentacene–porphyrin dyad **5** in a yield of 67% as a purple solid. Beginning with pentacene derivative **2**, the analogous procedure gave dyad **6** in 74% yield, also as a purple solid.

Both **5** and **6** were stable for weeks when stored as solids under ambient laboratory conditions. In solution, however, the pentacene–porphyrin dyads **5** and **6** were relatively unstable. The color of the solution changed from purple to red over a period of hours, even when protected from air and light, in accord with loss of the acene chromophore. This behavior is consistent with what we, and others [19], have observed in other pentacene systems, and the constitution of the decomposition product(s) was not pursued. This instability is disappointing, but not completely unexpected, as Stillmann and coworkers have demonstrated that the acene chromophore is destroyed rather rapidly in solution [17a], when porphyrins are appended to the *pro cata* positions of 6,13-diphenyl pentacene, likely through addition of oxygen [19].

3.4. *Characterization of pentacene–porphyrin dyads*

^{1}H NMR spectroscopy provides evidence for formation of the pentacene–porphyrin dyad **5** from pentacene **1** and porphyrin **3**. The ^{1}H NMR spectrum of **5** reflects the diamagnetic anisotropy from the aromatic porphyrin, as found for **4**. Specifically, the *ortho*-pyridyl protons of **5** are shifted to 2.42 ppm and 1.95 ppm, relative to uncomplexed **1**, in which they are found at 9.29 and 8.81 ppm, respectively (figure 4). Furthermore, the *meta*-proton

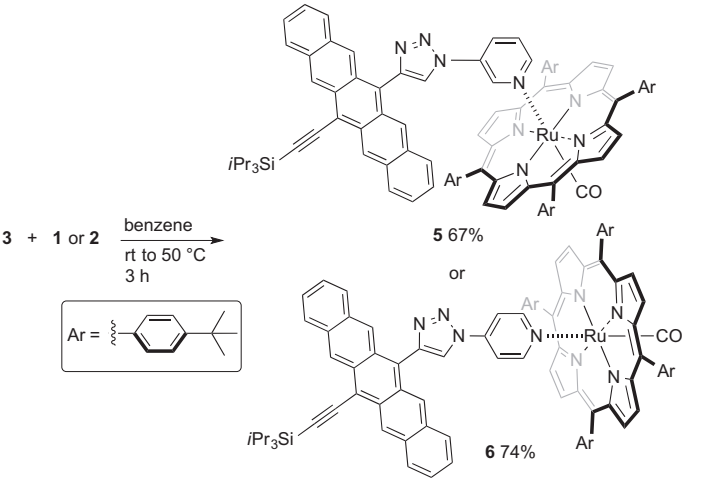

Scheme 2. Synthesis of pentacene–porphyrin dyads **5** and **6**.

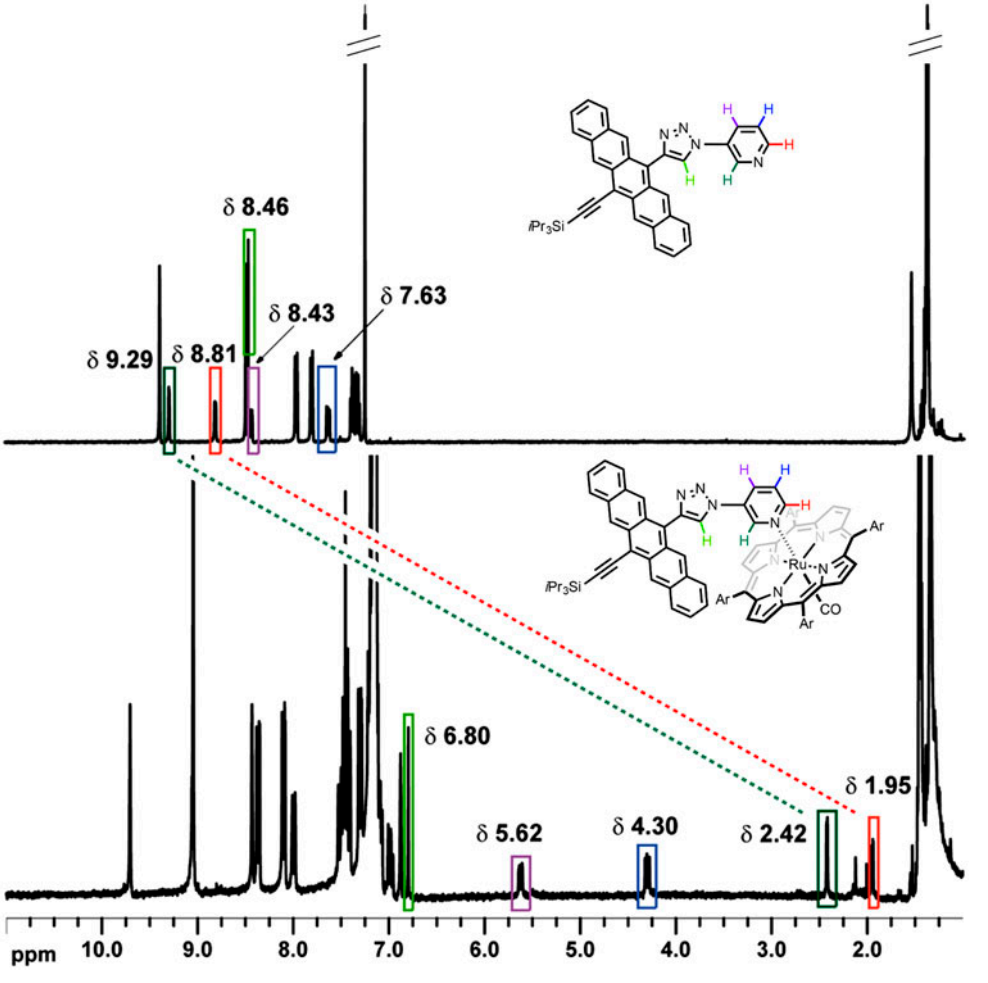

Figure 4. ^{1}H NMR spectra comparing chemical shifts of pentacene **1** (400 MHz, $CDCl_3$) and pentacene–porphyrin dyad **5** (300 MHz, C_6D_6). The resonances assigned to the pyridyl and triazole protons are highlighted (see http://dx.doi.org/10.1080/00958972.2015.1057711 for color version).

(7.63 ppm) and the *para*-proton (8.43 ppm) in **1** are shifted upfield upon coordination, and in dyad **5,** they are found at 4.30 ppm (*meta*-proton) and 5.62 ppm (*para*-proton). Even the triazole proton, which is found somewhat downfield at 8.46 ppm in pentacene **1** (but still in the typical range [16, 20], experiences the diamagnetic anisotropy from the porphyrin ring, and this proton is shifted upfield to 6.80 ppm in dyad **5**.

The spectral characterization of dyad **6** reflects similar trends as established for **5**. In the ^{1}H NMR spectrum of **2**, the pyridyl protons are doublets at 8.84 and 7.91 ppm, and the triazole proton resonates as a singlet at 8.48 ppm (figure 5). Upon coordination to Ru(II)-porphyrin **3**, the doublets from the pyridyl group of **6** shift dramatically upfield to 1.86 and 4.72 ppm, while the proton of the triazole ring shifts to 6.30 ppm (figure 5).

IR spectroscopic analyses of **5** and **6** are also consistent with the formation of the proposed supramolecular dyads. Although the shift in each complex is not always significant,

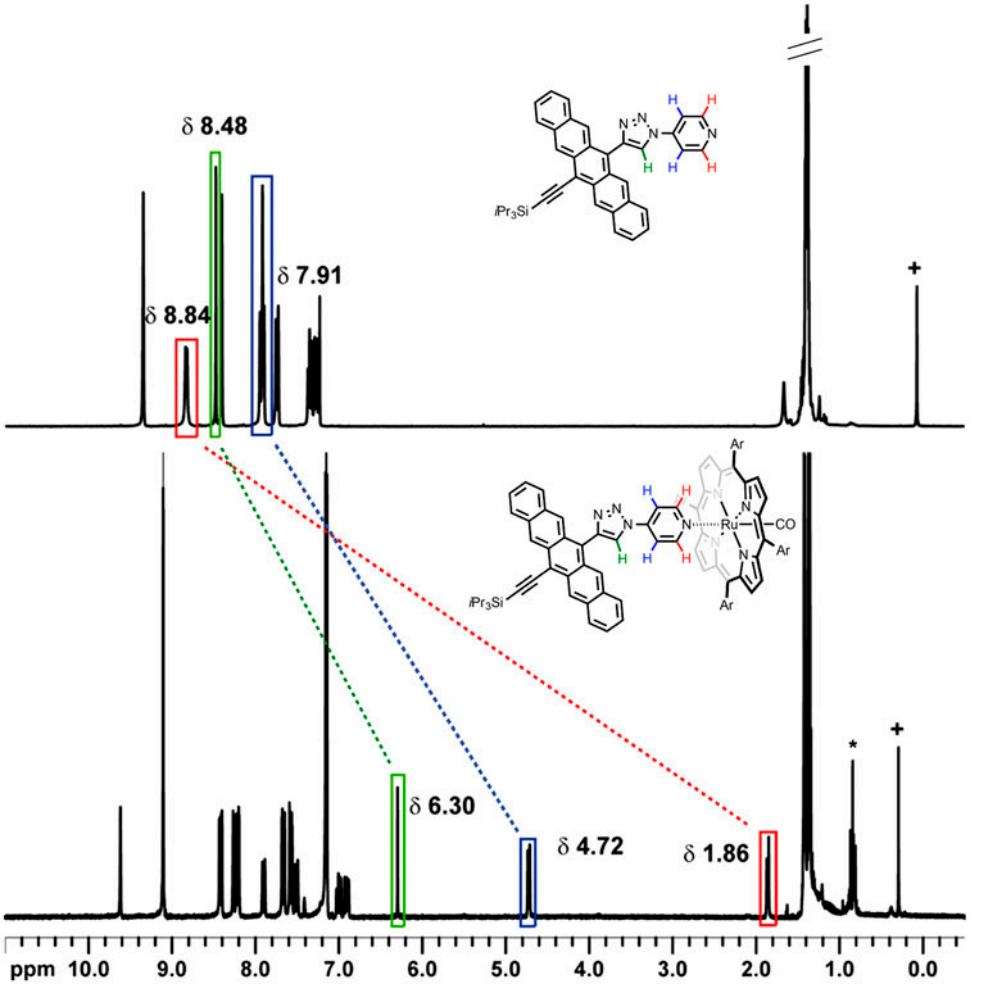

Figure 5. ^{1}H NMR spectra (300 MHz) comparing chemical shifts of pentacene **2** ($CDCl_3$) and dyad **6** (C_6D_6). The resonances assigned to the pyridyl and triazole protons are highlighted (+ = silicon grease and * = hexanes) (see http://dx.doi.org/10.1080/00958972.2015.1057711 for color version).

the vibrational band of the CO group moves from 1943 cm^{-1} for porphyrin **3** to 1949 cm^{-1} for **5** and to 1966 cm^{-1} for **6**, as shown in figure 6.

To some extent, solution-state UV–vis analysis sheds light on the electronic properties of the pentacene–porphyrin assemblies, and this has been investigated for the more stable of the two dyads, **5** (figure 7). In the UV region, pentacene **1** shows a strong absorption at 308 nm (ε = 240,000) along with a weak absorption at 348 nm. In the low energy region, absorption bands at 534, 574, and 621 nm are present. Pentacene–porphyrin dyad **5** shows a strong absorption centered at 309 nm (ε = 210,000) and a weak absorption at 346 nm, along with the strong Soret-band at 415 nm (ε = 200,000). The low energy region shows three absorption maxima at 534, 571, and 622 nm. Ultimately, the UV–vis spectrum of **5** demonstrates that there is little change to the electronic absorption properties of either the individual pentacene or porphyrin moieties, in comparison with dyad **5**. Thus, the

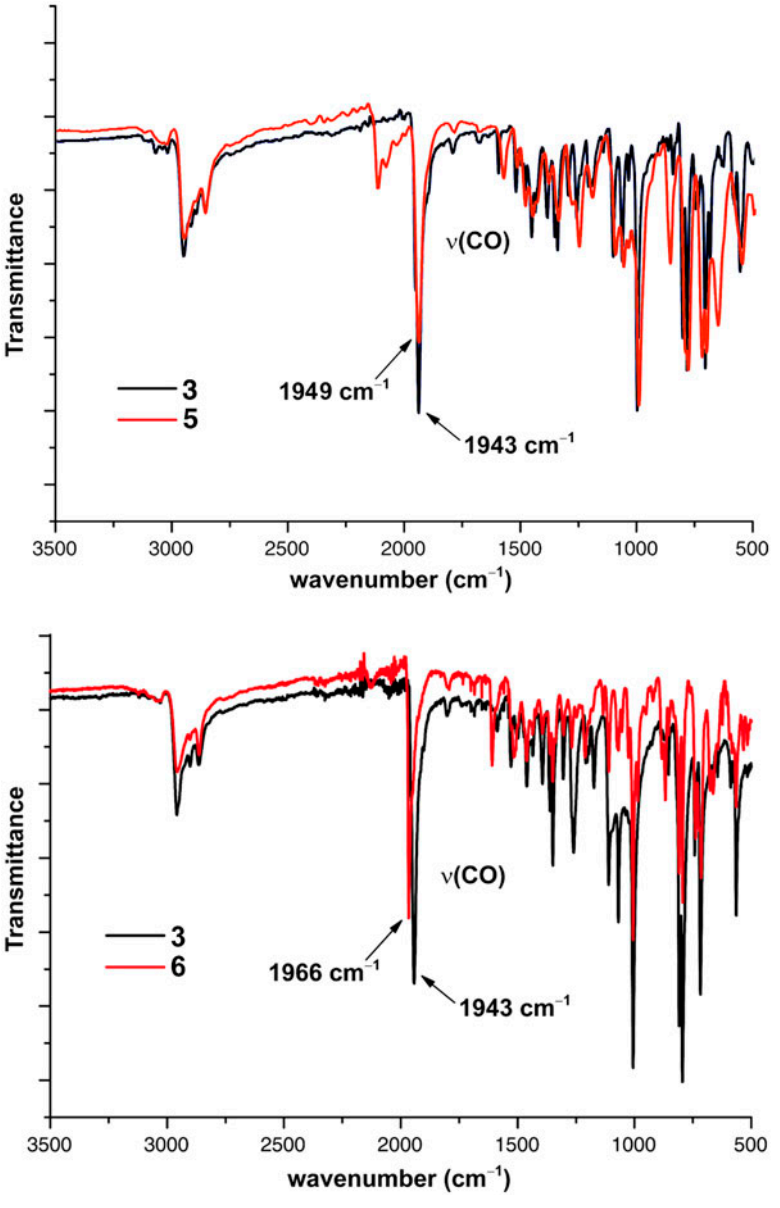

Figure 6. A comparison of the CO stretching vibration of **3** to **5** (top) and **3** to **6** (bottom).

absorption spectrum of **5** can, for the most part, be regarded as a summation of pentacene and porphyrin absorptions, and the same trend is true for the analysis of dyad **6**. It is worth noting, however, that, in the dyads, the absorptions of the porphyrin chromophore complement the absorptions of the pentacene groups, leading to a significant increase of absorptions in the mid-UV–vis range *versus* pentacene alone.

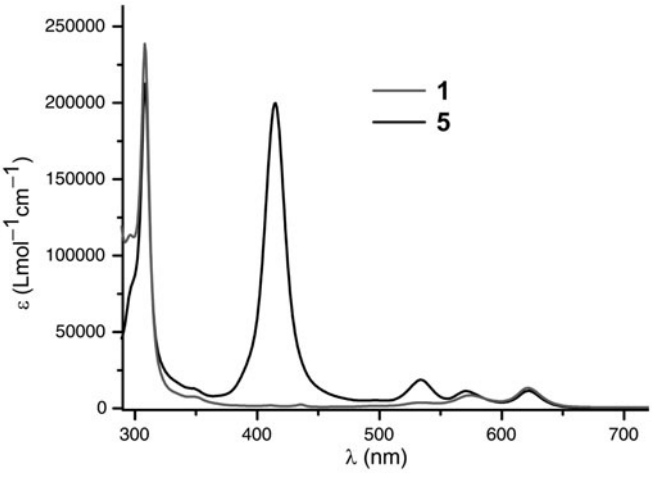

Figure 7. UV–vis spectra of **1** and of **5** as measured in CH_2Cl_2.

4. Conclusion

Axial coordination of pyridyl-containing pentacenes has been performed. The obtained pentacene–porphyrin dyads **5** and **6** are soluble in common organic solvents. The dyads **5** and **6** have been characterized through a combination of IR, NMR, UV–vis spectroscopy, and MS spectrometry and compared to the pyridyl-porphyrin model compound **3**. The UV–vis spectroscopic analysis reveals that the electronic properties of pentacenes are relatively unaffected by axial coordination to the porphyrin. Nevertheless, the UV–vis spectrum of, e.g. **5**, shows that the dyads cover a broad absorption range in the visible part of the UV–vis spectrum. This could be interesting for optoelectronic devices, although stability issues of pentacene–porphyrin dyads have to be considered, since solution-state stability for **5** and **6** is somewhat limited. Thus, the practical use of pentacene–porphyrin complexes in devices will likely require developing a structural motif that provides stabilization to the acene framework.

Disclosure statement

No potential conflict of interest was reported by the authors.

Funding

This work was supported by the Energie Campus Nürnberg (EnCN), "Solar Technologies go Hybrid" (an initiative of the Bavarian State Ministry for Science, Research and Art), and the Deutsche Forschungsgemeinschaft (DFG) through the Cluster of Excellence "Engineering of Advanced Materials".

References

[1] (a) G. de Ruiter, M. Lahav, M.E. van der Boom. *Acc. Chem. Res.*, **47**, 3407 (2014); (b) Y. Chi, B. Tong, P.-T. Chou. *Coord. Chem. Rev.*, **281**, 1 (2014); (c) P.K. Singh, V.K. Singh. *Pure Appl. Chem.*, **82**, 1845 (2010); (d) D.A. Thornton, *Coord. Chem. Rev.*, **104**, 251 (1990).

[2] (a) K. Campbell, R. McDonald, R.R. Tykwinski. *J. Porphyrins Phthalocyanines*, **9**, 794 (2005); (b) K. Campbell, R. McDonald, N.R. Branda, R.R. Tykwinski. *Org. Lett.*, **3**, 1045 (2001); (c) K. Campbell, R. McDonald, R.R. Tykwinski. *J. Org. Chem.*, **67**, 11 (2002).

[3] C.A. Hunter, R.K. Hyde. *Angew. Chem Int. Ed.*, **35**, 1936 (1996).

[4] E. Iengo, E. Zangrando, E. Alessio. *Acc. Chem. Res.*, **39**, 841 (2006). I. Bouamaied, T. Coskun, E. Stulz, *Struct. Bond.*, **121**, 1 (2006).

[5] I.-W. Hwang, T. Kamada, T.K. Ahn, D.M. Ko, T. Nakamura, A. Tsuda, A. Osuka, D. Kim. *J. Am. Chem. Soc.*, **126**, 16187 (2004).

[6] S. Fukuzumi, K. Saito, K. Ohkubo, V. Troiani, H. Qiu, S. Gadde, F. D'Souza, N. Solladié. *Phys. Chem. Chem. Phys.*, **13**, 17019 (2011).

[7] S.A. Ikbal, S. Brahma, S.P. Rath. *Inorg. Chem.*, **51**, 9666 (2012).

[8] F. Fages, J.A. Wytko, J. Weiss. *C.R. Chim.*, **11**, 1241 (2008).

[9] S. Brahma, S.A. Ikbal, S.P. Rath. *Inorg. Chim. Acta*, **372**, 62 (2011).

[10] D.R. Maulding, B.G. Roberts. *J. Org. Chem.*, **34**, 1734 (1969).

[11] J.E. Anthony. *Angew. Chem. Int. Ed.*, **47**, 452 (2008); J.E. Anthony. *Chem. Rev.*, **106**, 5028 (2006); J.E. Anthony, A. Facchetti, M. Heeney, S.R. Marder, X. Zhan, *Adv. Mater.*, **22**, 3876 (2010).

[12] D. Lehnherr, R.R. Tykwinski. *Aust. J. Chem.*, **64**, 919 (2011).

[13] M. Bendikov, F. Wudl, D.F. Perepichka. *Chem. Rev.*, **104**, 4891 (2004).

[14] J.W. Ward, Z.A. Lamport, O.D. Jurchescu. *ChemPhysChem*, **16**, 1118 (2015).

[15] C.W. Tornøe, C. Christensen, M. Meldal. *J. Org. Chem.*, **67**, 3057 (2002); V.V. Rostovtsev, L.G. Green, V.V. Fokin, K.B. Sharpless. *Angew. Chem Int. Ed.*, **41**, 2596 (2002).

[16] A.R. Waterloo, S. Kunakom, F. Hampel, R.R. Tykwinski. *Macromol. Chem. Phys.*, **213**, 1020 (2012).

[17] For examples of covalent structures combining porphyrins and pentacenes, see: (a) L. Jiang, J.T. Engle, R.A. Zaenglein, A. Matus, C.J. Ziegler, H. Wang, M.J. Stillman. *Chem. Eur. J.*, **20**, 13865 (2014); (b) C.-Y. Lin, Y.-C. Wang, S.-J. Hsu, C.-F. Lo, E.W.-G. Diau. *J. Phys. Chem. C*, **114**, 687 (2010); (c) K. Susumu, T.V. Duncan, M.J. Therien. *J. Am. Chem. Soc.*, **127**, 5186 (2005).

[18] For synthetic procedure, see: D.P. Rillema, J.K. Nagle, L.F. Barringer Jr, T.J. Meyer. *J. Am. Chem. Soc.*, **103**, 56 (1981); For characterization, see: K. Funatsu, T. Imamura, A. Ichimura, Y. Sasaki. *Inorg. Chem.*, **37**, 4986 (1998).

[19] S.S. Zade, M. Bendikov. *J. Phys. Org. Chem.*, **25**, 452 (2012).

[20] T. Luu, B.J. Medos, E.R. Graham, D.M. Vallee, R. McDonald, M.J. Ferguson, R.R. Tykwinski. *J. Org. Chem.*, **75**, 8498 (2010).